

Resonance Chiral Lagrangian Currents and Experimental Data for $\tau^- \rightarrow \pi^- \pi^- \pi^+ \nu_\tau$

I. M. Nugent

I. Physikalisches Institut B RWTH Aachen, D-52056 Aachen, Germany

T. Przedziński

*The Faculty of Physics, Astronomy and Applied Computer Science,
Jagellonian University, Reymonta 4, 30-059 Cracow, Poland*

P. Roig

*Instituto de Física, Universidad Nacional Autónoma de México,
AP 20-364, México D.F. 01000, México*

O. Shekhovtsova

*Kharkov Institute of Physics and Technology
61108, Akademicheskaya,1, Kharkov, Ukraine and
Institute of Nuclear Physics, PAN, Kraków, ul. Radzikowskiego 152, Poland*

Z. Wąs

*Institute of Nuclear Physics, PAN, Kraków, ul. Radzikowskiego 152, Poland and
CERN PH-TH, CH-1211 Geneva 23, Switzerland*

In this paper we document the modifications introduced to the previous version of the Resonance Chiral Lagrangian current (*Phys.Rev.* **D86** (2012) 113008) of the $\tau^\pm \rightarrow \pi^\pm \pi^\pm \pi^\mp \nu_\tau$ decay which enable the one dimensional distributions measured by the BaBar collaboration to be well modeled. The main change required to model the data is the addition of the σ resonance. Systematic errors, theoretical and experimental ones, limitations due to fits of one dimensional distributions only, and resulting difficulties and statistical/systematic errors for fitted parameters are addressed.

The current and fitting environment is ready for comparisons with the fully exclusive experimental data. The present result for $\tau^\pm \rightarrow \pi^\pm \pi^\pm \pi^\mp \nu_\tau$ is encouraging for work on other τ decay modes and Resonance Chiral Lagrangian based currents.

PACS numbers: 13.35.Dx, 12.39.Fe, 89.20.Ff, 87.55K-

I. INTRODUCTION

In our paper [1] we described an upgrade of the Monte Carlo generator TAUOLA using the results of the Resonance Chiral Lagrangian ($R\chi L$) for the τ lepton decay into the most important two and three meson channels. The necessary theoretical concepts were collected, numerical tests of the implementations were completed and documented. Finally, we presented strategy for fitting experimental data and the systematic uncertainties associated with the experimental measurement. However, there was and remain until now, an obvious limitation due to the fact that we are using one-dimensional projections of the invariant masses for a multi-dimensional distribution. The first comparison [2] of the $R\chi L$ results for the $\pi^- \pi^- \pi^+$ mode with the BaBar data [3], did not demonstrated a satisfactory agreement for the two pion invariant mass distributions. With the recent availability of the unfolded distributions for all invariant masses constructed from observable decay products for this channel [3], we found ourselves in an excellent position to work on model improvement for the $\pi^- \pi^- \pi^+$ mode. We would like to stress here that the choice of the three pion mode is not accidental. The kinematical configuration is complex and the three pion mode has the largest branching

ratio among the three meson decay modes. Moreover, this decay mode together with the decays into two pions, which are much easier to model, are a useful tool for spin-parity analysis of the recently discovered Higgs boson [4, 5] through its di- τ decays [6, 7].

Our paper is organized as follows. In Section 2 we present modifications to the currents previously prepared by us [1]. We give a brief motivation for the choice of selected extensions. In Section 3, we present numerical results and we discuss available options. Section 4 is devoted to documentation of our fitting approach, which could be substantially simplified thanks to availability of unfolded invariant mass distributions. In Section 5 we discuss systematic uncertainties for the fit resulting from statistical and systematic uncertainties of the experimental data. Some technical details of our set-up use are collected in this section as well. Summary, Section 6, closes the paper.

II. EXTENSION OF CURRENTS

For the final state of three pions π^- , π^- , π^+ with the momenta respectively p_1 , p_2 and p_3 , Lorentz invariance determines the decomposition of the hadronic current to

be [1]

$$J^\mu = N \left\{ T_\nu^\mu [(p_2 - p_3)^\nu F_1 - (p_3 - p_1)^\nu F_2] + q^\mu F_4 - \frac{i}{4\pi^2 F^2} c_5 \epsilon^{\mu\nu\rho\sigma} p_1^\nu p_2^\rho p_3^\sigma F_5 \right\}, \quad (1)$$

where: $T_{\mu\nu} = g_{\mu\nu} - q_\mu q_\nu / q^2$ denotes the transverse projector, and $q^\mu = (p_1 + p_2 + p_3)^\mu$ is the momentum of the hadronic system. Here F stands for the pion decay constant in the chiral limit. In the isospin symmetry limit, the F_5 form factor for the three pion mode is zero due to G -parity conservation [8] and thus we will neglect it.

Functions F_i , the hadronic form factors, depend in general on three independent invariant masses that can be constructed from the three meson four-vectors. We chose $q^2 = (p_1 + p_2 + p_3)^2$ and two invariant masses $s_1 = (p_2 + p_3)^2$, $s_2 = (p_1 + p_3)^2$ built from pairs of momenta. Then $s_3 = (p_1 + p_2)^2$ can be calculated¹ from the other three invariants and is $s_3 = q^2 - s_1 - s_2 + 3m_\pi^2$. The form of the hadronic current is the most general one and constrained only by Lorentz invariance. The normalization factor is $N = \cos\theta_{\text{Cabibbo}}/F$.

It is convenient to write down the hadronic form factors as

$$F_i = (F_i^X + F_i^R + F_i^{\text{RR}}) \cdot R^{3\pi}, \quad i = 1, 2, 4, \quad (2)$$

where F_i^X is the chiral contribution, F_i^R is the one resonance contribution and F_i^{RR} is the double-resonance part. The $R^{3\pi}$ constant equals 1 for $\pi^- \pi^- \pi^+$ (and -1 for $\pi^0 \pi^0 \pi^-$).

The exact form of the function F_i is presented in [1] eqs. (4)-(11). The comparison to data [2] hints that the lack of the $f_0(600)$ (or σ) meson contribution in our parameterization may be responsible for this discrepancy². The σ meson is, predominantly, a tetraquark state [11–13], and it cannot be included in the $R\chi L$ formalism³,

¹ In our approach the hadronic form factors are calculated in the isospin limit and $m_\pi = (m_{\pi^0} + 2m_{\pi^\pm})/3$.

² We would like to point out that the same problem was shown in the E791 analysis of the $D^+ \rightarrow \pi^+ \pi^+ \pi^-$ decays [9] (see also the FOCUS article [10]), where the σ contribution was modeled relying on a Breit-Wigner factor. In this case, the inclusion of the σ contribution is mandatory to describe the data, since it produces basically half of the decay width. The good agreement with data shown in [9] can be taken as a support of modeling the σ contribution by means of a Breit-Wigner, as it is done in this paper, see eq. (5), and can be considered as phenomenologically sufficiently sound solution till we have better based parameterization.

³ In addition to the abovementioned $D^+ \rightarrow \pi^+ \pi^+ \pi^-$ decays, the σ meson has been observed to play an important role in $\pi\pi$ scattering [12, 14, 15], and it has also been relevant for the understanding of the $J/\Psi \rightarrow \omega\pi\pi$ and $\Psi(2S) \rightarrow J/\Psi\pi\pi$ decays [16, 17]. However further investigation of its effect in processes with the same hadronic final states, as the one considered in this paper, is required. See our discussion on the fit to the experimental data including σ and other alternatives, as Coulomb interaction, in section III and the paper summary.

which is devised for ordinary $q\bar{q}$ resonances⁴. The inclusion of rescattering effects of this kind is an involved task from the computational point of view, even in the case of scalar amplitudes [22, 23]. In view of this we have decided to incorporate the σ meson following a more phenomenological approach, more specifically, a simple extension of the one used by CLEO [24]. This effect is included into the $F_1(Q^2, s, t)$ and $F_2(Q^2, s, t)$ form factors in the following way

$$F_1^R \rightarrow F_1^R + \frac{\sqrt{2}F_V G_V}{3F^2} [\alpha_\sigma B W_\sigma(s_1) F_\sigma(q^2, s_1) + \beta_\sigma B W_\sigma(s_2) F_\sigma(q^2, s_2)], \quad (3)$$

$$F_1^{\text{RR}} \rightarrow F_1^{\text{RR}} + \frac{4F_A G_V}{3F^2} \frac{q^2}{q^2 - M_{a_1}^2 - iM_{a_1}\Gamma_{a_1}(q^2)} [\gamma_\sigma B W_\sigma(s_1) F_\sigma(q^2, s_1) + \delta_\sigma B W_\sigma(s_2) F_\sigma(q^2, s_2)], \quad (4)$$

where

$$B W_\sigma(x) = \frac{M_\sigma^2}{M_\sigma^2 - x - iM_\sigma\Gamma_\sigma(x)}, \quad (5)$$

$$\Gamma_\sigma(x) = \Gamma_\sigma \frac{\sigma_\pi(x)}{\sigma_\pi(M_\sigma^2)}, \quad (6)$$

$$F_\sigma(q^2, x) = \exp\left[\frac{-\lambda(q^2, x, m_\pi^2)R_\sigma^2}{8q^2}\right], \quad (7)$$

and $\sigma_\pi(q^2) \equiv \sqrt{1 - 4m_\pi^2/q^2}$ and $\lambda(x, y, z) = (x - y - z)^2 - 4yz$. Bose symmetry implies that the form factors F_1 and F_2 are related $F_2(q^2, s_2, s_1) = F_1(q^2, s_1, s_2)$. As a consequence the hadronic current (1) is symmetrical under exchange of s_1 and s_2 . The main differences between the σ meson parameterization, eqs. (3) to (7), and the one used by CLEO can be summarized as:

- there is one resonance contribution (F_1^R) in (3) whereas the CLEO parameterization contains only the double resonance contributions (F_1^{RR}). The presence of the one resonance diagrams is a feature of $R\chi L$ (and other Lagrangian approaches), for discussion see Section 7 of [1];
- $\alpha_\sigma \neq \beta_\sigma$ and $\gamma_\sigma \neq \delta_\sigma$, no symmetry requirement enforces these equalities in equation (3). In contrary, CLEO Collaboration [24] uses the simplified case where vertices $a_1 \rightarrow \sigma\pi$ and $\sigma \rightarrow \pi\pi$ are assumed to be constant and $\alpha_\sigma = \beta_\sigma$ and $\gamma_\sigma = \delta_\sigma$;
- the CLEO Collaboration fixed both the σ mass and its width to the values predicted by the Tornqvist unitarized quark model [25] whereas we fit these parameters.

⁴ The $q\bar{q}$ assignment for the lightest axial-vector mesons is favored within the $R\chi L$ approach [18], see however Refs. [19–21].

The width for the $\tau^- \rightarrow \pi^- \pi^- \pi^+ \nu_\tau$ decay can be written down in the terms of the hadronic form factors in Eqs. (2) and (3)

$$\frac{d\Gamma}{dq^2} = \frac{G_F^2 |V_{ud}|^2}{128(2\pi)^5 M_\tau F^2} \left(\frac{M_\tau^2}{q^2} - 1 \right)^2 \int ds_1 ds_2 \left[W_{SA} + \frac{1}{3} \left(1 + 2 \frac{q^2}{M_\tau^2} \right) W_A \right], \quad (8)$$

where

$$\begin{aligned} W_A &= -(V_1^\mu F_1 + V_2^\mu F_2 + V_3^\mu F_3) \\ &\quad (V_{1\mu} F_1 + V_{2\mu} F_2 + V_{3\mu} F_3)^*, \\ W_{SA} &= q^2 |F_4|^2. \end{aligned} \quad (9)$$

The following phase space integration limits have to be used

$$\int ds_1 ds_2 = \int_{4m_\pi^2}^{(\sqrt{q^2} - m_\pi)^2} ds_1 \int_{(s_2)_-}^{(s_2)_+} ds_2, \quad (10)$$

where

$$\begin{aligned} (s_2)_\pm &= \frac{1}{4s} \left\{ (q^2 - m_\pi^2)^2 \right. \\ &\quad \left. - [\lambda^{1/2}(q^2, s_1, m_\pi^2) \mp \lambda^{1/2}(m_\pi^2, m_\pi^2, s_1)]^2 \right\}. \end{aligned} \quad (11)$$

The Coulomb interaction can be important near the production threshold. We use the far-field approximation; the final-state pions are treated as stable point-like objects and the three pion interaction is treated as a superposition of the two pion ones. The corresponding invariant masses (we have attractive interaction for the pion pairs of the invariant masses s_1 and s_2 and the repulsive interaction for the s_3) define the strength of the pair interactions. The two pion system can be in S or P-wave state. To estimate the Coulomb interaction in S-wave we can apply the results of Section 94 of Ref. [26] which changes the differential decay width as follows

$$\frac{d\Gamma}{dq^2 ds_1 ds_2} \rightarrow \frac{d\Gamma}{dq^2 ds_1 ds_2} \frac{2\alpha\pi/v_0(s_1)}{1 - \exp[-2\alpha\pi/v_0(s_1)]} \frac{2\alpha\pi/v_0(s_2)}{1 - \exp[-2\alpha\pi/v_0(s_2)]} \frac{2\alpha\pi/v_0(s_3)}{\exp[2\alpha\pi/v_0(s_3)] - 1}, \quad (12)$$

where in r.h.s. $d\Gamma$ is the S-wave part of the differential decay width (see eq. 8) neglecting the Coulomb interactions, $v_0(s)$ is the relative velocity of two pions in the two pion system with invariant mass s , i.e. $v_0(s) = 2\sigma_\pi(s)/(1 + \sigma_\pi^2(s))$, where $\sigma_\pi(s)$ is defined below eq. (5). Precision studies of the two-pion vector form factor (see e.g. [27] and references therein), more specifically, a P-wave two pion state, did not require to include the Coulomb interaction between the pion pair to describe the data accurately. We will consequently neglect P-wave Coulomb interaction among the final-state pions

and stick to formula (12) to evaluate the effect of electromagnetic interactions among the pions and set (8) on r.h.s. of (12).

The a_1 width can be written down as the imaginary part of the two-loop axial-vector-axial-vector correlator with suitable flavour indices [28]

$$\begin{aligned} \Gamma_{a_1}(q^2) &= 2\Gamma_{a_1}^\pi(q^2)\theta(q^2 - 9m_\pi^2) \\ &\quad + 2\Gamma_{a_1}^{K^\pm}(q^2)\theta(q^2 - (m_\pi + 2m_K)^2) \\ &\quad + \Gamma_{a_1}^{K^0}(q^2)\theta(q^2 - (m_\pi + 2m_K)^2), \end{aligned} \quad (13)$$

where

$$\Gamma_{a_1}^{\pi,K}(q^2) = \frac{S}{192(2\pi)^3 F_A^2 F^2 M_{a_1}} \left(\frac{M_{a_1}^2}{q^2} - 1 \right)^2 \int ds dt W_A^{\pi,K} \quad (14)$$

stands for the contribution from the individual three-pion [28] and two kaons - one pion [29] absorptive cuts. As similar integrands are present in eq. (8) for the partial decay width of τ to three pions and in eq. (13) for the q^2 -dependent a_1 width, we could use this property to simplify the code for calculating the invariant mass spectra and profit in full from the unfolded invariant mass distribution of BaBar which recently became public [3]. The Monte Carlo simulations could be avoided and we could use semi-analytical functions in fits.

We would like to stress that we neglect, in our numerical analysis, the σ contribution on r.h.s of Eq. (14), which should be suppressed in the large- N_C counting. We will come to discussion of additional ambiguities related to the σ contribution in the Summary.

III. NUMERICAL RESULTS

The parameters of the current⁵ described in the previous Section were used in a fit as it is discussed in Section IV. The σ contribution is switched on by setting `FF3PISCAL = 2` in `value_parameter.f`. The numerical values of the model parameters are collected in Table I, the goodness of the fit⁶ is quantified by $\chi^2/ndf = 6658/401$. We discuss next our best fit numerical results; the plots of invariant masses are given

⁵ The widths of the ρ and a_1 resonances, $\Gamma_\rho \equiv \Gamma_\rho(M_\rho^2)$ and $\Gamma_{a_1} \equiv \Gamma_{a_1}(M_{a_1}^2)$, are not fit parameters and are calculated by means of eq. (29) in [1] and eq. (13).

⁶ In our previous paper, χ^2 was computed using the combined statistical and systematic uncertainties since only the total covariance matrix was publicly available. For the present results we obtain $\chi^2/ndf = 910/401$ when the total covariance matrix is used and conditions enabling direct comparisons are fulfilled. This is eight times better than the previous result [2]. The spectra [3] used now and in Ref. [2] have different binnings. In particular, [3] uses a bin width of 10 MeV while Ref. [2] used a 20 MeV bin width. Moreover, the current spectra have smaller uncertainties that are reduced relative to the results of Ref. [30].

	M_ρ	$M_{\rho'}$	$\Gamma_{\rho'}$	M_{a_1}	M_σ	Γ_σ	F	F_V
Min	0.767	1.35	0.30	0.99	0.400	0.400	0.088	0.11
Max	0.780	1.50	0.50	1.25	0.550	0.700	0.094	0.25
Fit	0.771849	1.350000	0.448379	1.091865	0.487512	0.700000	0.091337	0.168652
	F_A	$\beta_{\rho'}$	α_σ	β_σ	γ_σ	δ_σ	R_σ	
Min	0.1	-0.37	-10.	-10.	-10.	-10.	-10.	
Max	0.2	-0.17	10.	10.	10.	10.	10.	
Fit	0.131425	-0.318551	-8.795938	9.763701	1.264263	0.656762	1.866913	

TABLE I: Numerical ranges of the $R\chi L$ parameters used to fit the BaBar data for three pion mode [3]. The approximate uncertainty estimates are collected in Table III. The $M_{\rho'}$ and Γ_σ best fit values are observed to be at the boundary of the physically motivated range of variation that we allowed for them. The $M_{\rho'}$ value may be lower than expected because of missing resonances found in [24]. On the contrary, Γ_σ appears to be high because of its strong correlation with R_σ . This correlation, however, does not show up in Table IV because its evaluation is not reliable for parameters lying on the boundary of the allowed parameter space.

in Fig. 1 and in Fig. 2. The partial width resulting from the phase space integration of the matrix element $\Gamma_{\tau^- \rightarrow \pi^- \pi^- \pi^+ \nu_\tau} = 1.9974 \cdot 10^{-13}$ GeV agrees with the one measured by BaBar $\Gamma = (2.00 \pm 0.03\%) \cdot 10^{-13}$ GeV [31] and its PDG value $\Gamma = (2.04 \pm 0.01\%) \cdot 10^{-13}$ GeV [16]⁷.

These results can be confronted with those obtained previously without the σ contribution, which can be found in Table 2 of [1].

The effects of the electromagnetic interaction among the final-state pions, see (12), is turned on by setting `FCOUL = 1` in `value_parameter.f`. Taking into account the Coulomb interaction (when the σ contribution was not included) we obtained⁸ a $\chi^2/ndf = 33225/401$. Therefore, the Coulomb interaction without the σ contribution cannot describe the data in the low-energy region. The effect on the total width is about 2%, if Coulomb interaction is introduced for currents with parameters set as in Table I. When it is introduced at the time of fit the effect is even smaller. It is also negligible for the one-dimensional distributions, the χ^2 changes by 2% if Coulomb interaction is switched on during the fitting procedure, for both the cases with and without the σ contribution.

A. Case of $\pi^0 \pi^0 \pi^-$ mode

A current analogous to eq.(3) can be written for the $\pi^0 \pi^0 \pi^-$ mode too. In this case the neutral pions may be

produced by the σ meson, exchanged in s_3 :

$$F_1^R \rightarrow F_1^R + \frac{\sqrt{2}F_V G_V}{3F^2} \alpha_\sigma^0 B W_\sigma(s_3) F_\sigma(q^2, s_3), \quad (15)$$

$$F_1^{RR} \rightarrow F_1^{RR} + \frac{4F_A G_V}{3F^2} \frac{q^2}{q^2 - M_{a_1}^2 - iM_{a_1} \Gamma_{a_1}(q^2)} \gamma_\sigma^0 B W_\sigma(s_3) F_\sigma(q^2, s_3).$$

The form factors F_1^R, F_1^{RR} in r.h.s. are the same as for the $\pi^- \pi^- \pi^+$ mode (up to a common overall sign, see eq.(4) of [1]) whereas no symmetry requirement implies that the σ contribution for the $\pi^0 \pi^0 \pi^-$ decay channel coincides with the corresponding one in the $\pi^- \pi^- \pi^+$ mode. We would like to stress that the analysis of CLEO supports the idea that the value of the σ vertex parameters are different for $\pi^0 \pi^0 \pi^-$ and $\pi^- \pi^- \pi^+$ modes, see Tables 2 and 3 in [24].

To obtain results for $\pi^0 \pi^0 \pi^-$, we have used the following solution. The parameters of the σ : $\alpha_\sigma, \gamma_\sigma, R_\sigma, M_\sigma$ and Γ_σ were fitted again to the $\pi^- \pi^- \pi^+$ data, varying in the same range as in the default fit, see Table I. All three spectra of invariant masses and width were used as experimental input to the fit. However, the additional approximation $\alpha_\sigma = \beta_\sigma, \gamma_\sigma = \delta_\sigma$, necessary for extension to the $\pi^0 \pi^0 \pi^-$ mode, was used. The fit gives⁹

$$\alpha_\sigma = 1.139486, \quad \gamma_\sigma = 0.889769, \quad (16)$$

$$R_\sigma = 0.000013, \quad M_\sigma = 0.550, \quad \Gamma_\sigma = 0.700.$$

Using the results of this fit¹⁰, we may estimate the α_σ^0

⁷ We quote the branching ratio excluding $\tau^- \rightarrow \pi^- \bar{K}^0 \nu_\tau$, with the subsequent decay $K_S^0 \rightarrow \pi^+ \pi^-$. The $R\chi L$ current for the three pion mode, see Section 2.1 of [1], does not include the feed down from this mode. The value measured by BaBar also excludes the \bar{K}^0 contributions. The effect of $\tau^- \rightarrow \pi^- \omega \nu_\tau$, followed by $\omega \rightarrow \pi^+ \pi^-$ is numerically negligible (branching ratio $\sim 3 \cdot 10^{-4}$) and is excluded from our current as well.

⁸ Note that this result cannot be directly compared with the result from our previous paper as in this case a different χ^2 function (that takes into account correlation between histogram bins) is used.

⁹ Obviously, this constrained fit for $\pi^- \pi^- \pi^+$ is worse than for the values provided in Table I (χ^2/ndf for the new minimum is 21589/401). However, when the new fit is performed with all other parameters allowed to vary within the ranges mentioned in the Table I, and only with the assumption $\alpha_\sigma = \beta_\sigma, \gamma_\sigma = \delta_\sigma$, the corresponding minimum gives $\chi^2/ndf = 8707/401$ which is closer to our default result for $\pi^- \pi^- \pi^+$ channel. The results of this fit are collected in Table II. They provide another hint that the σ contribution to our decays may be considered as a not fully confirmed and/or understood phenomenon.

¹⁰ Note that two of the parameters are at the limits we requested

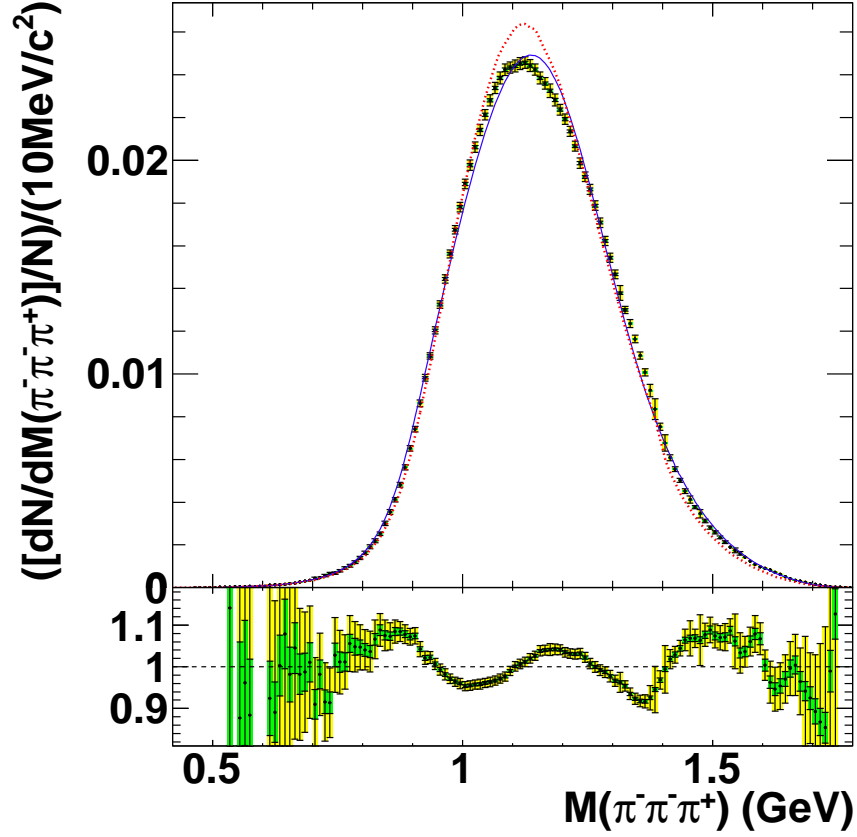


FIG. 1: The differential decay width of the $\tau^- \rightarrow \pi^- \pi^- \pi^+ \nu_\tau$ channel is plotted versus the invariant mass distribution of the three pion system. The BaBar measurements [3] are represented by the data points, with the results from the $R_{\chi L}$ current as described in the text (blue line) and the old tune from CLEO from Refs. [32, 33] (red-dashed line) overlaid. At the bottom of the figure, ratio of new $R_{\chi L}$ prediction to the data is given. The parameters used in our new model are collected in Table I.

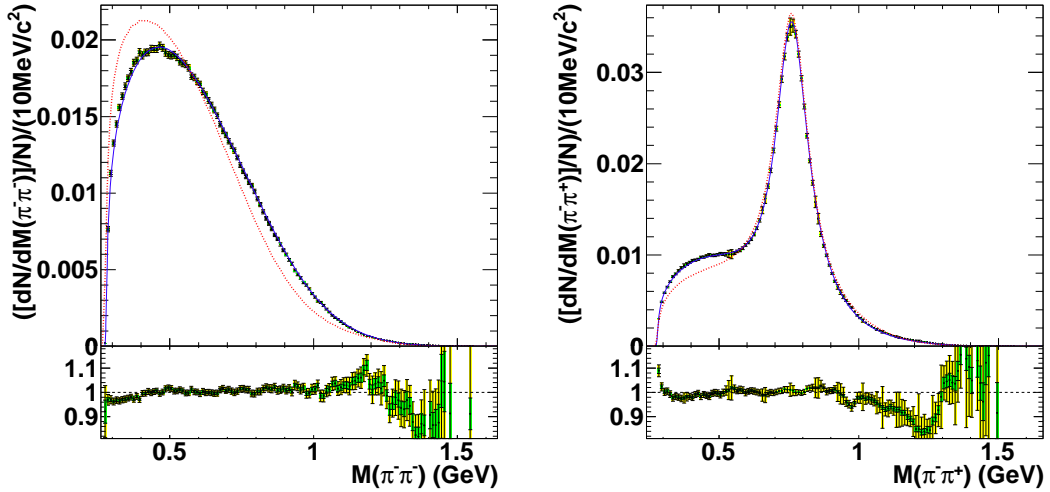


FIG. 2: The $\tau^- \rightarrow \pi^- \pi^- \pi^+ \nu_\tau$ decay invariant mass distribution of the two-pion pairs. The BaBar measurements [3] are represented by the data points, with the results from the $R_{\chi L}$ current as described in the text (blue line) and the old tune from CLEO from Refs. [32, 33] (red-dashed line) overlaid. At the bottom of the figures ratio of new $R_{\chi L}$ prediction to the data is given. The parameters used in our new model are collected in Table I.

and γ_σ^0 parameters for the $\pi^0\pi^0\pi^-$ mode

$$\begin{aligned}\alpha_\sigma^0 &= \alpha_\sigma \cdot \text{Scaling}_{factor}^\gamma \\ \gamma_\sigma^0 &= \gamma_\sigma \cdot \text{Scaling}_{factor}^\gamma\end{aligned}$$

employing the result for the $a_1 \rightarrow \sigma\pi$ constant vertex from Tables 3 and 4 of [24]. We find $\text{Scaling}_{factor}^\gamma = 2.1/3.35 = 0.63$. Therefore, for the $\pi^0\pi^0\pi^-$ channel we obtain $\alpha_\sigma^0 = 0.63 \cdot 1.139486$, $\gamma_\sigma^0 = 0.63 \cdot 0.889769$, $R_\sigma = 0.000013$, $M_\sigma = 0.55$ and $\Gamma_\sigma = 0.7$. All other constants remain¹¹ as in Table I; we obtain the $\pi^0\pi^0\pi^-$ partial width¹² $\Gamma = (2.1211 \pm 0.016\%) \cdot 10^{-13}$, 1% higher than the central PDG value and within the errors cited by PDG. When all model parameters are adopted in the fit (see Table II), and once the scaling factor is again included, the $\pi^0\pi^0\pi^-$ partial width becomes $\Gamma = (2.2706 \pm 0.016\%) \cdot 10^{-13}$ GeV. That is 8.1% higher than the PDG value¹³.

The fit results in eq. (16) reproduce the PDG width of the $\pi^0\pi^0\pi^-$ mode better than those in Table II. This is possibly a consequence of accidental partial cancellation of phase space effect and the effect of assumption $\alpha_\sigma = \beta_\sigma$, $\gamma_\sigma = \delta_\sigma$ which is not supported theoretically for the three charged pion mode. However, it is needed to obtain an estimate of the α_σ and γ_σ parameters in the $\pi^0\pi^0\pi^-$ channel for which no data are available. We propose the results of eq. (16) for the σ parameters and for the others as given in Table I (i.e. as for the $\pi^-\pi^-\pi^+$ mode) for default, until the $\pi^0\pi^0\pi^-$ experimental distributions or other improvements become available for the fit.

IV. FITTING STRATEGY

For the purpose of fitting, a set of semi-analytic distributions over s_1 , s_3 and q^2 has been prepared. In the three-dimensional distribution of formula (9), two of the parameters are integrated over¹⁴. A change of integration

¹¹ We would like to draw attention to the fact that both fits, this one and the one in Table II, prefer an R_σ value consistent with zero. This coincides with the CLEO result [24, 34].

¹² This was calculated by setting the parameter $\text{BRA1} = 0$ in routine `INITDK`. Results are taken from sample of $2 \cdot 10^6$ events.

¹³ We note that there is a $\sim 2.4\%$ difference between the $\pi^-\pi^-\pi^+$

variable was introduced to smoothen the integrand and improve integration convergence. The 16-point Gaussian integration routine from the old Fortran CERNLIB was used. Two options were interchanged. In the first integration adopts the number of divisions for integration domain by itself to fulfill the precision requirement. In the second case the number of divisions has to be provided by the user. Even though the second method is less sophisticated, it is better suited for fitting algorithms, where minuscule changes of integrals due to variation of model parameters are of primary importance. For all of these methods, a C wrappers have been written and the interface for work with ROOT [35] has been prepared.

The a_1 width is written down as in eq. (13). However, its computation, through a double integration for every q^2 is demanding on CPU time. To speed up the calculation, at first, we simply calculated a_1 width as a function of q^2 once and we kept it in a table, even though it should be re-calculated whenever parameters of the model were changed (see Section 4 and Tab. 4 of Ref. [1] for technical details). This approximation was largely insufficient. Later for the dominant 3π contribution to the a_1 width ($\Gamma_{a_1}^\pi$ in (13)) we followed the method used for a long time since year 1992 [8]: the a_1 width is calculated by (14) at several values of q^2 only, for other values, it is replaced with the polynomial extrapolation $g(q^2)$ given by eq. (17). The coefficients a, b, c, d, e, f, g, h, p, which appear in (17), are calculated from the set of equations where the l.h.s. of (17) is fixed to the three pion part of the a_1 width calculated from eq. (13).

For the sub-dominant $KK\pi$ contribution to the a_1 width a table (see Section 4 and Tab. 4 of Ref. [1] for technical details) is produced, and it is not recalculated with the changing fit parameters at every step of the fit iteration. It was checked that the above simplifications did not bring substantial effects for the final results.

We have used the following form for $g(q^2)$, inspired from Ref. [36]:

and $\pi^-\pi^0\pi^0$ branching ratios due to phase-space as a consequence of the π^0 mass being smaller than the π^\pm mass.

¹⁴ For the future application of the fitting procedure a set of two-dimensional distributions has been prepared as well.

$$g(q^2) = \begin{cases} (q^2 - 9m_\pi^2)^3(a - b(q^2 - 9m_\pi^2) + c(q^2 - 9m_\pi^2)^2), & 9m_\pi^2 < q^2 < (M_\rho + m_\pi)^2, \\ q^2(d - e/q^2 + f/q^4 - g/q^6), & (M_\rho + m_\pi)^2 < q^2 < 3(M_\rho + m_\pi)^2, \\ h + 2p \frac{q^2 - 3(M_\rho + m_\pi)^2}{(M_\rho + m_\pi)^2}, & 3(M_\rho + m_\pi)^2 < q^2 < m_\tau^2, \end{cases} \quad (17)$$

where from the best fit we have obtained

$$\begin{aligned}a &= 1.54712, \quad b = 3.83256, \quad c = 4.52798, \quad d = 0.30997, \\ e &= 1.56106, \quad f = 3.73605, \\ g &= 2.00856, \quad h = 0.38688, \quad p = -0.00108,\end{aligned}$$

and M_ρ can be taken as the PDG $\rho(770)$ mass and m_π as an isospin averaged mass.

As in Ref. [8] the expansion in r.h.s. of (17) starts from $(q^2 - 9m_\pi^2)^3$ to reproduce the P-wave phase space. The

	M_ρ	$M_{\rho'}$	$\Gamma_{\rho'}$	M_{a_1}	M_σ	Γ_σ	F	F_V
Min	0.767	1.35	0.30	0.99	0.400	0.400	0.088	0.11
Max	0.780	1.50	0.50	1.25	0.550	0.700	0.094	0.25
Fit	0.772774	1.350000	0.410404	1.116400	0.495353	0.465367	0.089675	0.167130
	F_A	$\beta_{\rho'}$	α_σ	γ_σ	R_σ			
Min	0.1	-0.37	-10.	-10.	-10.			
Max	0.2	-0.17	10.	10.	10.			
Fit	0.146848	-0.301847	1.094981	0.582533	0.000315			

TABLE II: Numerical values of the $R\chi L$ parameters fitted to BaBar data for three charged pion mode [3] requiring $\alpha_\sigma = \beta_\sigma$, $\gamma_\sigma = \delta_\sigma$. The approximate uncertainty estimates from `minuit` are 0.4 for R_σ , 0.13 for $M_{\rho'}$ and below 10^{-2} for rest of the parameters.

difference for the q^2 -dependent a_1 width calculated as the sum of (17) and the $KK\pi$ table and the precise results is less than 7% starting from $q^2 = 0.293 \text{ GeV}^2$. It decreases below 1% starting from $q^2 = 1.1 \text{ GeV}^2$, where it is of major importance. For q^2 below M_ρ^2 numerical values for $g(q^2)$ are small, thus of no numerical consequences for the calculated currents.

Once our numerical integration algorithms were understood and the speed of the calculation improved, we could use for the a_1 width formula (13) and re-tabulate in the manner described in Section 4 of ref [1], whenever parameters of the model were changed in the fit algorithm; parallelization was useful.

In our fits we have used a set of three one-dimensional distributions from BaBar [3]. We normalize the BaBar data to its branching ratio taken also from the BaBar measurements [31] ($\Gamma = 2.0 \cdot 10^{-13} \text{ GeV}$) and perform a χ^2 fit using `minuit` from the `ROOT` library. The covariance matrix provided by BaBar already assumes the statistical uncertainties are Gaussian¹⁵. The χ^2 minimized in the fit is determined as the sum of χ^2 from the three one-dimensional distributions, where correlations between the histograms have been neglected. The fitting function has been designed in the following way:

- A set of three histograms is generated using the aforementioned semi-analytic distributions.
- For each X for which `minuit` requests function value, an appropriate bin content is returned.
- Whenever `minuit` changes one of the parameters:
 - TAUOLA is reinitialized with a new set of parameters.
 - The a_1 width formula is pre-tabulated¹⁶.
 - A new set of histograms is generated.

Without complete re-tabulation of a_1 width, calculating each step took less than a minute on a 2.8GHz processor. It has been further improved by parallelization of the histogram generation. This has been done by submitting each bin of each of the three histograms as a separate task distributed evenly among all cores assigned to the job. This reduced the time for one step to 6-8 seconds on a 8 core 2.8GHz processor. This approach allows for flexible assignment of the number of cores used for computation¹⁷.

Retabulation increases computation time only twice. The χ^2 for such a case is about 10% smaller. For the final steps of the fits we also include integration over the bin width, instead of previously used value at the bin center. This makes χ^2 smaller by another 5-6% at a cost of 3 to 5 times slower computation. When both options are included and fits are performed from the point calculated without these improvements, the χ^2 is reduced yet again by 5% to 6%. Nonetheless such improvements do not change the results in a significant manner, except parameters of the σ . This points to the unconfirmed nature of the σ or the insensitivity of the decay of the σ without the availability of the angular correlations.

Our results collected in section III, in particular Figs. 1 and 2, have been obtained with both a_1 retabulation and integration of bin width taken into account.

V. DISCUSSION OF UNCERTAINTIES FOR THE FIT

After having completed the presentation of our results, rather good agreement with the data has been found,

width (eq. (17)) was reinitialized. It was then used instead of a_1 table during histogram generation.

¹⁵ Because the BaBar covariance matrix was constructed using systematic uncertainties that were estimated with Toy MC, there are statistical fluctuations that cause instabilities in the matrix inversion. Therefore, a cut-off on the magnitude of the correlations was used. The value of the cut-off was determined from where the χ^2 , as a function of the cut-off value, becomes unstable.

¹⁶ During first fits, at this point the function for interpolation of a_1

¹⁷ Note that this method can also be extended to use multiple processors. However, from our tests the total amount of cores used shouldn't exceed 24. Above this threshold the communication between the main program and the child processes slows down the whole calculation giving no gain in time. This could be solved by introducing more than one main program but we decided against further optimization of the code as the calculation time was good enough for our purposes.

substantially better than available in the literature. Let us turn our attention to the possible systematic uncertainties resulting from the use of experimental data available at this moment. Our currents used in the fits are not constructed posterior to fit properties related to the shapes of the distributions but are the results of theoretical assumptions. We will cover these points in the following subsections.

A. Numerical Results and Statistical Uncertainties

The parameters obtained from our fit are collected in Table III. The corresponding correlation matrix can be found in Table IV. The statistical uncertainties were determined using the `HESSE` routine from `minuit` [37] under the assumption that the correlations between distributions and the correlations related to having two entries per event in the $\pi^- \pi^+$ distribution can be neglected. We find a strong correlation (correlation coefficients moduli bigger than 0.95) between the parameters

$$M_{a_1}, F_\pi, F_V, \beta_{\rho'}.$$

There are also large correlations (with coefficients larger than 0.85) between these parameters and β_σ and $\Gamma_{\rho'}$. The correlations between these two last parameters and the former set with α_σ and M_ρ are only slightly smaller. The Γ_σ is uncorrelated because the Hessian Matrix is not computed correctly for parameters that have a minimum on the boundary.

Some of the previously commented correlations are related to the underlying dynamics of the process, as we explain in the following.

The dominant contribution to the amplitude originates from the exchange $a_1 \rightarrow (\rho; \rho')\pi$. The explicit form of the form factors F_i^{RR} ($i = 1, 2$) is given in eqs. (6-11) of Ref. [1]. Since in eq. (3) we use $G_V = F_\pi^2/F_V$, see discussion in Section 7 of Ref. [1], the factor multiplying the a_1 propagator¹⁸ is $G_V \cdot F_A/F_\pi^3 = F_V \cdot F_A/F_\pi$. As a consequence, strong correlations between F_V , F_A , F_π and also M_{a_1} and $\beta_{\rho'}$ could have been expected, as it is the case for all of them but for F_A which shows slightly smaller correlations. It could also be guessed that correlations affected the other $\rho - \rho'$ parameters (M_ρ and Γ'_ρ), as are indeed observed; but we could not find a reason why strong correlations affect also the α_σ and β_σ parameters but not the other parameters entering our model of the σ contributions (γ_σ , δ_σ and R_σ).

As we will see later in the paper, for example in the next sub-section on the discussion of systematic errors for our results, there are further correlations between parameters of the model, which are difficult to understand. This underlines the importance of the systematic uncertainties

of our data. The actual position of the minimum obtained in our fit may be to some degree an artifact and result from systematic effects from the measurements which can be accounted for with systematic and statistical uncertainties. This is important specially for the numerical values of strongly correlated parameters. Before the analysis of multi-dimensional distributions is available for us in the future, let us review the possible consequences of the systematic uncertainties of the data.

B. Systematic uncertainties of the data

The experimental systematic uncertainties were taken into account using Toy MC Studies. This approach was adopted instead of studying individual uncertainties to demonstrate that systematic uncertainties for the invariant mass measured by Belle and BaBar can be easily and correctly incorporated into an analysis. The disadvantage of this method is that one can not isolate the impact of individual uncertainties and the uncertainties are assumed to be Gaussian. These limitations are intrinsic to the invariant mass spectra made available by these collaborations. The Toy MC was generated under the Gaussian assumption using Cholesky Decomposition on the systematic covariance matrix provided by the BaBar experiment to include the correlations. The fit was re-run for 100 Toy MC to estimate the impact on the experimental systematic uncertainties. The resulting systematic uncertainties are presented in Table III, while the correlation matrix for the fit parameters can be read from Table V. From Table III, it can be seen that the extraction of the fit parameters is limited by the systematic uncertainties. The main systematic uncertainties are related to: the limited MC statistics used in the BaBar analysis; the modeling of the detector response for the reconstructions of the invariant masses, namely the resolution, scale for the momentum and angles of the measured particle as well as the bias of the unfolding procedure; and the modeling of the backgrounds. The uncertainty associated with the limited MC statistics, which is comparable to the statistical error on the data, is one of the most significant components of the total systematic uncertainty. The other main systematic uncertainties impact the shape of the invariant mass spectra. The most important one is the detector modeling. As one would expect the uncertainty related to the modeling of the detector response is most pronounced where the rate of change in the mass spectra is large. This uncertainty is of particular importance for determining the width of resonances or parameters correlated to those widths. The main backgrounds come from the π^0 fake rate associated with the $\tau^- \rightarrow \pi^- \pi^- \pi^+ \pi^0 \nu_\tau$ events and cross-feed from $\tau^- \rightarrow K^- \pi^- \pi^+ \nu_\tau$. The $\tau^- \rightarrow h^- h^- h^+ \nu_\tau$ cross-feed from particle mis-identification is primarily found in the low Q^2 region from 0.7 – 0.9 GeV and the $\pi^- \pi^+$ region below the ρ resonance. The $\tau^- \rightarrow \pi^- \pi^- \pi^+ \pi^0 \nu_\tau$ is most significant around the low Q^2 region and the low

¹⁸ The $1/F_\pi$ factor was factored out in the normalization of the currents, see eq. (1).

Parameter	number	Value
α_σ	0	$-8.(795938) \pm (0.023) \pm 5$
β_σ	1	$9.(763701) \pm 0.(013) \pm 4.0$
γ_σ	2	$1.2(64263) \pm 0.0(09) \pm 0.8$
δ_σ	3	$0.6(56762) \pm 0.0(06) \pm 1.1$
R_σ	4	$1.8(66913) \pm 0.0(053) \pm 1.4$
M_ρ	5	$0.7718(49) \pm 0.0001(8) \pm 0.0033$
$M_{\rho'}$	6	$1.35(00001) \pm (9 \cdot 10^{-6}) \pm 0.06$
$\Gamma_{\rho'}$	7	$0.44(8379) \pm 0.00(6) \pm 0.06$
M_{a_1}	8	$1.091(865) \pm 0.00(029) \pm 0.014$
M_σ	9	$0.48(7512) \pm 0.00(033) \pm 0.05$
Γ_σ	10	$0.70(0) \pm (2.23 \cdot 10^{-05}) \pm 0.21$
F_π	11	$0.0913(37) \pm (3.3 \cdot 10^{-5}) \pm 0.0019$
F_V	12	$0.1686(52) \pm 0.0001(8) \pm 0.0080$
F_A	13	$0.131(425) \pm (6 \cdot 10^{-5}) \pm 0.011$
$\beta_{\rho'}$	14	$-0.318(551) \pm 0.000(9) \pm 0.034$

TABLE III: The fit parameters presented with the statistical and systematic uncertainties. The numbers in round brackets enclose digits that are not significant according to the (other) errors.

	α_σ	β_σ	γ_σ	δ_σ	R_σ	M_ρ	$M_{\rho'}$	$\Gamma_{\rho'}$	M_{a_1}	M_σ	Γ_σ	F_π	F_V	F_A	$\beta_{\rho'}$
α_σ	1	0.60	0.36	-0.29	-0.41	-0.69	0.46	0.68	-0.77	-0.09	0.02	0.78	0.76	0.52	-0.78
β_σ	0.60	1	0.44	-0.39	-0.42	-0.75	0.55	0.79	-0.89	-0.16	0.04	0.89	0.88	0.58	-0.88
γ_σ	0.36	0.44	1	-0.56	-0.22	-0.59	0.16	0.37	-0.47	-0.28	0.00	0.49	0.45	0.30	-0.45
δ_σ	-0.29	-0.39	-0.56	1	0.46	0.46	-0.24	-0.42	0.49	0.01	0.01	-0.49	-0.47	-0.31	0.47
R_σ	-0.41	-0.42	-0.22	0.46	1	0.42	-0.33	-0.56	0.62	0.34	0.02	-0.53	-0.56	-0.42	0.48
M_ρ	-0.69	-0.75	-0.59	0.46	0.42	1	-0.27	-0.64	0.79	0.29	-0.02	-0.83	-0.74	-0.48	0.75
$M_{\rho'}$	0.46	0.55	0.16	-0.24	-0.33	-0.27	1	0.67	-0.61	-0.13	0.03	0.61	0.66	0.37	-0.65
$\Gamma_{\rho'}$	0.68	0.79	0.37	-0.42	-0.56	-0.64	0.67	1	-0.88	-0.24	0.03	0.86	0.88	0.57	-0.88
M_{a_1}	-0.77	-0.89	-0.47	0.49	0.62	0.79	-0.61	-0.88	1	0.28	-0.03	-0.96	-0.97	-0.62	0.95
M_σ	-0.09	-0.16	-0.28	0.01	0.34	0.29	-0.13	-0.24	0.28	1	-0.02	-0.30	-0.29	-0.20	0.30
Γ_σ	0.02	0.04	0.00	0.01	0.02	-0.02	0.03	0.03	-0.03	-0.02	1	0.03	0.03	0.03	-0.04
F_π	0.78	0.89	0.49	-0.49	-0.53	-0.83	0.61	0.86	-0.96	-0.30	0.03	1	0.95	0.55	-0.97
F_V	0.76	0.88	0.45	-0.47	-0.56	-0.74	0.66	0.88	-0.97	-0.29	0.03	0.95	1	0.63	-0.96
F_A	0.52	0.58	0.30	-0.31	-0.42	-0.48	0.37	0.57	-0.62	-0.20	0.03	0.55	0.63	1	-0.56
$\beta_{\rho'}$	-0.78	-0.88	-0.45	0.47	0.48	0.75	-0.65	-0.88	0.95	0.30	-0.04	-0.97	-0.96	-0.56	1

TABLE IV: The statistical correlation matrix from `minuit` for the fit parameters presented to two decimal places.

$\pi^-\pi^+$ invariant mass. Since this is the region where the σ is added to improve the agreement of the fit with data, the systematic uncertainties are essential to interpret the magnitude of the disagreement and quantifying the level at which the $R\chi L$ approach breaks down. The $q\bar{q}$ background is negligible for most of the invariant mass spectra except at the high Q^2 above 1.5 GeV. The Bhabha background, although negligible over most of the phase space, does have a significant contribution to the low Q^2 region, up to 0.8 GeV, and the high- Q^2 region above 1.6 GeV as well as below 0.3 GeV in the $\pi^-\pi^-$ spectra. Parameters which are coupled to features that have a significant contribution to the spectra, for example the ρ mass, have systematic uncertainties corresponding to the naive expectation from the known scale, resolution uncertainties and fit bias uncertainties on the distribution. For other parameters, the conclusions are less clear due to the sensitivity in the one-dimensional spectra and strong correlations. For example, the uncertainties associated with the mass and width of the $a_1(1260)$ and $\rho'(1450)$ are dependent on $\rho(770)$ mass, width and coupling parameters. However, it should be noted that these parameters are likely biased and will not correspond to physically meaningful values due to missing resonance structures that have been reported in [24, 34].

C. Test of the convergence of the fitting procedure and Gaussian Approximation

To verify that our fitting procedure does not depend on the starting choice of numerical values for the parameters, and that it converges properly to a single minimum, we have ran fits from several different starting points. The procedure of this test is as follows:

- A random scan of the parameter space has been performed: sample of 210K random points has been tested and the χ^2 of the difference between these points and data have been stored¹⁹.
- The sample have been sorted by the χ^2 and a thousand best results have been selected.
- From these results, 20 points have been selected in a way that maximizes the distance between these points.

¹⁹ Since for this purpose the size of the sample is more important than the quality of the result, we were able to make use of the interpolation formula (17) (described in Section IV) instead of dense pretabulation of a_1 width. We have also neglected integration over bin width. These simplifications introduced bias for χ^2 calculation which only weakly depends on the actual choice of the model parameters. However, thanks to this, we have gained a factor of 7 in speed of calculation, which greatly increased the sample size.

- From these points we perform a full fit to the data using a method that takes into account the correlation between bins in the histograms.

We have observed that more than 50% of the results converge to the minimum described in this paper²⁰. This is an important test that indicates our results are stable and indicates that our fitting procedure converges properly regardless of the choice of the starting point.

The Gaussian approximation used for the statistical uncertainty is validated using two toy MC studies. For one of the tests we have used the parameter values for the current minimum of the fit to generate 8 Monte Carlo samples of 20 MEvents. We then proceed to fit our currents to these samples as if they were experimental data samples with the errors scaled to match the statistics in the data. The first test started the fit from the very same values used for generation of the samples. This is to check how our fitting procedure behaves close to the minimum and how the statistical error of the experimental sample affects the result. The results are consistent with the starting values. In the second test, we used the default starting values from our previous paper [1]. The result of the fit is in good agreement with the values used for generation of Monte Carlo samples. This indicates that the errors are within the regime where the Gaussian approximation for the uncertainties is valid. We assume that any bias from the correlations is negligible.

D. Pole position of the ρ , ρ' and σ resonances

We presented our best fit results for the $R\chi L$ parameters with statistical and systematic uncertainties in Table III. It may be desirable, however, to give the corresponding resonance pole mass and width parameters, which are model independent, to allow for comparisons with other works and encode the spectrum features in physically meaningful parameters. We are aware, though, that the complex dynamics of the process under study prevents a competitive determination of the ρ , ρ' and σ resonance parameters, whose pole positions can be determined with higher accuracy in $\pi\pi$ scattering and the vector two pion form factor, the latter either in e^+e^- scattering or τ decays.

Specifically, in order to obtain the corresponding physical mass and width one should compute the position of the pole in the second Riemann sheet of the complex s plane, say s_{pole} . One has (see Refs. [38–40] for the prescriptions on how to deal with the cuts in the complex

²⁰ In other cases either `minuit` does not converge due to number of parameters being at their limit or converges to other local minima. This verifies our assumption that the fitted function has several minima. It does, however, point out that the minimum described in this paper has a very high chance of being a global minimum of this function as all other minima have distinguishably higher χ^2 .

	α_σ	β_σ	γ_σ	δ_σ	R_σ	M_ρ	$M_{\rho'}$	$\Gamma_{\rho'}$	M_{a_1}	M_σ	Γ_σ	F_π	F_V	F_A	$\beta_{\rho'}$
α_σ	1	-0.84	-0.27	-0.15	0.62	0.00	0.47	0.05	0.56	0.17	-0.61	-0.05	0.07	0.86	0.03
β_σ	-0.84	1	0.42	0.29	-0.77	-0.12	-0.37	-0.27	-0.64	-0.3	0.83	0.03	0.19	-0.55	-0.03
γ_σ	-0.27	0.42	1	-0.45	0.01	-0.47	-0.24	0.06	-0.37	0.03	0.23	-0.21	-0.04	-0.04	-0.11
δ_σ	-0.15	0.29	-0.45	1	-0.73	0.64	-0.15	-0.17	-0.04	-0.68	0.52	-0.26	0.68	-0.05	0.53
R_σ	0.62	-0.77	0.01	-0.73	1	-0.37	0.39	0.29	0.4	0.5	-0.79	0.21	-0.5	0.39	-0.32
M_ρ	0.00	-0.12	-0.47	0.64	-0.37	1	-0.26	0.05	0.15	-0.63	0.06	-0.5	0.48	-0.04	0.52
$M_{\rho'}$	0.47	-0.37	-0.24	-0.15	0.39	-0.26	1	-0.38	0.29	0.23	-0.32	0.35	-0.06	0.44	-0.07
$\Gamma_{\rho'}$	0.05	-0.27	0.06	-0.17	0.29	0.05	-0.38	1	0.29	0.08	-0.29	-0.24	-0.28	-0.07	0.06
M_{a_1}	0.56	-0.64	-0.37	-0.04	0.4	0.15	0.29	0.29	1	0.2	-0.56	-0.22	-0.2	0.55	0.5
M_σ	0.17	-0.3	0.03	-0.68	0.5	-0.63	0.23	0.08	0.2	1	-0.32	0.37	-0.67	-0.03	-0.34
Γ_σ	-0.61	0.83	0.23	0.52	-0.79	0.06	-0.32	-0.29	-0.56	-0.32	1	-0.03	0.44	-0.44	0.19
F_π	-0.05	0.03	-0.21	-0.26	0.21	-0.5	0.35	-0.24	-0.22	0.37	-0.03	1	-0.18	-0.17	-0.51
F_V	0.07	0.19	-0.04	0.68	-0.5	0.48	-0.06	-0.28	-0.2	-0.67	0.44	-0.18	1	0.24	0.5
F_A	0.86	-0.55	-0.04	-0.05	0.39	-0.04	0.44	-0.07	0.55	-0.03	-0.44	-0.17	0.24	1	0.18
$\beta_{\rho'}$	0.03	-0.03	-0.11	0.53	-0.32	0.52	-0.07	0.06	0.5	-0.34	0.19	-0.51	0.5	0.18	1

TABLE V: The correlation matrix for systematic uncertainties on the fit parameters presented to 2 decimal places.

functions entering the corresponding propagators)

$$\sqrt{s_{\text{pole}}} = M_{\rho}^{\text{pole}} - \frac{i}{2}\Gamma_{\rho}^{\text{pole}}. \quad (18)$$

If this procedure is carried on for the ρ , ρ' and σ resonances²¹ the results displayed in Table VI are obtained.

This kind of analysis is mandatory for the $f_0(500)$ and $\rho(770)$ resonance, for which the determination of its pole parameters has become an area of precision calculations. In particular there is very nice agreement in the literature for the $\rho(770)$ pole parameters: $M_{\rho}^{\text{pole}} = 761 \pm 3$ MeV and $\Gamma_{\rho}^{\text{pole}} = 145 \pm 4$ MeV using different types of data and methods (see [27] and references therein for details). Our value in Table VI, $s_{\rho}^{\text{pole}} = (760 \pm 4 - \frac{i}{2}(157_{-9}^{+7}))^2$ MeV² is compatible both for the mass and width, although the last value appears slightly large. We believe that this may be the result of the degeneracies and instabilities of the fit caused by the model used for the σ . In the case of the $\rho(1450)$ resonance, the comparison of our results in Table VI with those in Ref. [27] show agreement for the width but some tension on the mass that is 20 MeV smaller in Table VI. It is important to note here, that there are observed resonances, $f_2(1270)$ and $f_0(1370)$, which were reported CLEO [24, 34] and are suggested by the fit to the BaBar data. These additional resonances and the correlations between the ρ and ρ' parameters in the fits may also have affected the pole parameters of these resonances. Therefore, until these problems have been solved, the pole values for the masses and widths for the σ , ρ and ρ' may be of limited use.

After a long-standing debate about the existence of the σ , it is well-established now and the state-of-the-art dispersive analyses of $\pi\pi$ scattering data [12, 15, 41, 42] agree within a few MeV for the pole position of the σ around $((459_{-15}^{+25}) - i(279 \pm 30))$ MeV. Although with less precision, the results obtained using $D^+ \rightarrow \pi^+\pi^+\pi^-$ data, $s_{\sigma}^{\text{pole}} \sim (0.47 - i0.22)^2$ GeV² [43], are in reasonable agreement with the previous values, although with a smaller width. Our figures in Table VI, $s_{\sigma}^{\text{pole}} = (0.57 \pm 0.09 - i(0.31 \pm 0.08))^2$ GeV², are in accord with the more precise determinations obtained analyzing $\pi\pi$ scattering data. Despite this result supports the consistency of our picture where the role of the σ in the examined decays is manifest (specially in the decay distribution at low values of the $\pi^+\pi^-$ invariant mass) we judge that it is still too early to claim this as a confirmed fact and we would like to see if this trend is kept analyzing the complete multi-dimensional data set and/or improving the model of the σ contribution and possibly adding the missing, for example the $a_1(1640)$ resonance exchange, as it is discussed in the conclusions. We are

thus confident that in future stages of our work, when multi-dimensional distributions will be available for fits we shall be able to improve the determination of the poles associated to the resonances whose exchange dominates the $\tau^- \rightarrow (\pi\pi\pi)^-\nu_{\tau}$ decays.

E. Technical details

For the above applications to be possible we had to adapt TAUOLA library. Let us document the necessary changes.

The following FORTRAN functions with one, two and three-dimensional distributions have been prepared. Note that all of these functions have been also defined in `demo-fit/wid3pi_demo.h` for use in C/C++ environment. All of the parameters and return values of these functions are DOUBLE PRECISION.

- **FUNCTION FFWD3PI(QQ,S1,S3)**
Input: QQ = $m_{\pi^-\pi^-\pi^+}^2$, S1 = $m_{\pi^-\pi^+}^2$, S3 = $m_{\pi^-\pi^-}^2$. Returns $d\Gamma(\tau^- \rightarrow \pi^-\pi^-\pi^+\nu_{\tau})/(dQQdS1dS3)$. If QQ S1 S3 are outside of the phase space, this function returns zero.
- **FUNCTION DGAMS3QQ(QQ)**
FUNCTION DGAMS1QQ(QQ)
Calculates $\tau^- \rightarrow \pi^-\pi^-\pi^+\nu_{\tau}$ width as function of f(QQ,S3) and f(QQ,S1). The second parameter of the calculation is hidden in common block EXTERNAL. The definition in `demo-fit/wid3pi_demo.h` also includes the wrappers for these functions that handle the hidden parameter.
- **FUNCTION DGAMS1(XS1B)**
FUNCTION DGAMS3(XS3B)
FUNCTION DGAMQQ(XQQB)
These functions calculate $\tau^- \rightarrow \pi^-\pi^-\pi^+\nu_{\tau}$ width as function of S1, S3 or QQ using formula (2), (3), limits of integration are in (10).

To run the example program, it is required that ROOT is installed and its configuration is available through `root-config`.

- Compile TAUOLA-FORTRAN library by executing `make` in `TAUOLA-FORTRAN/tauola`.
- Compile additional libraries by executing `make` in `TAUOLA-FORTRAN/demo-standalone`.
- Compile example by executing `make` in `TAUOLA-FORTRAN/demo-fit`.
- Execute `./wid3pi_demo.exe` in `TAUOLA-FORTRAN/demo-fit`.

The program should return output:

²¹ The corresponding calculation for the a_1 resonance is beyond the scope of this paper, since the relevant three-meson cuts include the ρ and ρ' widths under a double integration making this determination rather cumbersome.

Resonance	$R\chi L$ (GeV) Mass	$R\chi L$ Width (GeV)	Pole Mass (GeV)	Pole Width (GeV)
$f_0(500)$	0.48 ± 0.05	0.70 ± 0.21	0.57 ± 0.09	0.61 ± 0.16
$\rho(770)$	0.772 ± 0.003	0.149 ± 0.007	0.760 ± 0.004	$0.157^{+0.007}_{-0.009}$
$\rho(1450)$	1.35 ± 0.06	0.44 ± 0.06	1.24 ± 0.05	0.37 ± 0.05

TABLE VI: $R\chi L$ and pole resonance masses and widths (in GeV) for the $f_0(500)$, $\rho(770)$ and $\rho(1450)$ resonances corresponding to our best fit results in Table III including statistical and systematic uncertainties. The $R\chi L$ $\rho(770)$ width is given in terms of F_π and M_ρ (see Ref. [1]).

```
Last integration variable QQ:total width of tau= ...
Last integration variable S1:total width of tau= ...
Last integration variable S3:total width of tau= ...
Calculating h12 (DGAMS3) ...
Calculating h13_23 (DGAMS1) ...
Calculating h123 (DGAMQQ) ...
```

where the total widths depend on the options and parameters used for computation. Additionally, output file `out.root` should be present with the histograms `h12`, `h13_23` and `h123` containing the distributions `S3`, `S1` (combined with `S2`) and `QQ` correspondingly.

This is a basic example used mostly as a technical test of numerical integration. It shows how the semi-analytic distributions can be accessed from the C++ program, and how they can be used to produce the histograms for comparison with the data. It also shows how fit parameters can be modified. It can be used as a starting point for further analysis or for writing new fitting algorithm.

The main fitting algorithm is located in subdirectory `TAUOLA/tauola/fitting`. As the algorithm itself is not a focus of this paper, its detailed description will be omitted. For users interested in more details we refer to `README` inside this directory for instructions on how to run the main program and how to use the algorithms provided. We refer to header files for documentation of the details of their use. We would like to point out that, as reiterated in `TAUOLA/fitting/README`, this code is not standalone and requires properly formatted data files which are not part of the distribution.

Finally let us point that the tar-ball of software distribution which includes code for the present work would also include code for unfinished work on other τ decay modes such as $KK\pi\nu_\tau$. That is why, at present, we plan to distribute the tar-ball upon request only.

VI. SUMMARY

In the present paper we have documented modification of the Resonance Chiral Theory currents for $\tau^- \rightarrow \pi^- \pi^- \pi^+ \nu_\tau$ decay of reference [1], necessary for agreement with the experimental data. The choice of this channel was motivated by its relatively large branching ratio, availability of unfolded experimental distribution and already non-trivial dynamics of three-pion final state. In addition, this channel is important for Higgs spin-

parity studies through the associated di- τ decays. Previously missing contribution from the σ resonance was added to our currents and final state Coulomb interactions were taken into account. As a result, we improved agreement with the data by a factor of about eight. Remaining differences are well below uncertainties expected for the $R\chi L$ currents approach. This is the first case when agreement for a non-trivial τ decay channel was obtained between the BaBar data [3] and the theoretical model. These comparisons allow for future precision tau decays Physics studies [44].

The agreement with data has improved, mainly, due to the inclusion of the σ meson, which is outside the $R\chi L$ approach. In Tables I and III, it can be seen that the value of Γ_σ is at the boundary. This appears to be the result of a numerical instability in the phenomenological description of the σ caused by the correlation between the R_σ in the exponential decay, equation 6, and with width of the Breit-Wigner, equation 4. This problem can only be resolved with a better parametrization of the σ which is currently not available to us²². Without the σ contribution the $R\chi L$ demonstrates only slightly better agreement with data than the CLEO model [2], Fig.1. Therefore, we cannot exclude that fits of similar good quality could be obtained if further work was done on the CLEO model²³. However, the $R\chi L$ approach ensures that the results for all hadronic currents reproduce the chiral limit of QCD at least up to next-to-next-to-leading order²⁴. In contrast, the phenomenological approximation, as it was done at CLEO, do not do that [46, 47]. We will come back to this point in our future analysis of the $KK\pi$ modes.

²² Parametrization following more rigorous lines like in Refs. [22, 23] requires some work on theoretical side and preferably multi-dimensional distributions for fits. We postpone such improvement for the next step of the work.

²³ It may be interesting to re-do the fits using old models. Such test may provide more insight on the predictive power of $R\chi L$ approach.

²⁴ It is a consequence of the fact that the inclusion of resonances is done using a Lagrangian, which is built requiring the known chiral symmetry breaking of QCD, the discrete symmetries of the strong interaction and unitary symmetry for the resonance fields, without any ad-hoc dynamical assumption [49]. Similar discussion for the two pion and $K\pi$ decay modes can be found in Refs. [27, 45].

Even though this work is based on one dimensional unfolded experimental distributions, we think that it is an important step forward. We have enriched our fitting arrangements, to profit from the availability of invariant mass distributions. Use of unfolded distributions and our technical arrangements substantially improved the speed of our fitting. We have implemented solutions based on parallel calculations.

The $R\chi L$ currents are ready for comparison with data for other τ decay channels and for work when unfolded multi-dimensional distributions are used. This may constrain the set of parameters obtained from fit to the $\tau^\pm \rightarrow \pi^\pm \pi^\pm \pi^\mp \nu_\tau$ channel, which features strong correlations. There exist other solutions (local minima) for the parameters which give somewhat worse agreement with the experimental data. It is worth mentioning that for the results of final fit the `minuit` `HESSE` method evaluates some elements of the correlation matrix to surpass 0.9.

An alternative approach, using linear approximation of the dependence on fitted parameters (described in Ref. [1]), is pursued independently [48]. It may become useful in later phases of the project. It has an advantage that it allows for experimental cuts to be introduced into the fitted distributions. It is, however, much slower and features instabilities if the choice of the fitted function is poor. It provides, however, independent test of our numerical methods used in the paper. In the present paper a simpler fitting method has been used as the unfolded distributions from experimental data are now available [3].

Discrepancies in the high mass region of the $\pi^+\pi^-$ invariant mass indicate the possibility of missing resonances in our $R\chi L$ approach. This is consistent with the observation of additional resonances, more specifically the $f_2(1270)$ and $f_0(1370)$, by CLEO in [24, 34]. Around 975 MeV, there is another discrepancy between the model and the data that suggests the presence of the $f_0(980)$ resonance²⁵. Although we could add phenomenologically the contribution of these resonances to the amplitude, we prefer not to do it at the moment to keep a compromise between the number of parameters, the stability of the fit and the amount of experimental data. We also comment below on the need to include the contribution of the $a_1(1640)$ resonance. It should be pointed out that the necessity of the σ in our model may be an artifact caused either by neglecting the dynamics associated with these additional resonances²⁶ or by the crudeness

of our σ parameterization. The largest discrepancies between data and the fitted distribution, which are responsible for a significant part of the total χ^2 , are observed in the 3π invariant mass distributions. The slope and shape of the disagreement in the 3π invariant mass spectra, in particular around 1.5 GeV in Fig. 1, indicates the possibility of interference between $a_1(1260)$ and its excited state $a_1(1640)$. The disagreement in the low mass regions around 1.0 GeV and below could be the result of a bias in the fit caused by leaving out the additional resonance. Although we currently restrict ourselves to the lowest axial-vector resonance, $a_1(1260)$, in future analysis of multi-dimensional distributions we are going to include the $a_1(1640)$ in the same way as it was done for the $\rho'(1450)$ to test our hypothesis²⁷. We prefer not to do this at the moment because the improvement of the fit on the peak and tail regions in the three-meson invariant mass distribution will come again together with an increase of the fit instability and a growth of the correlations between the (larger number of) fit parameters. Lacking the complete multi-dimensional distributions it is advisable to proceed this way at present. CLEO has also suggested a hint of a possible contribution of the pseudo-scalar resonance $\pi'(1300)$, which they have excluded at the $(1.0 - 1.9) \times 10^{-4}$ level with a 90% CL[24, 34]. This is below the current sensitivity of our fit. Finally, we note that previous dedicated studies within the $R\chi L$ framework [28, 46] did not obtain an improved description of the data when including the chiral logarithms [50]. This question could also be readdressed when more exclusive data will become available.

This paper represents a significant improvement in the agreement between our model and the data. The resulting fit parameters are substantially improved and are reasonable from the point of view of internal consistency of $R\chi L$. The obtained value for the a_1 mass can be used for the future theoretical study.

Predictions for the $\pi^0\pi^0\pi^-$ are obtained from the ones for $\pi^-\pi^-\pi^+$ directly with the help of isospin symmetry without any modifications except the part of σ contribution which was adapted and constraints from CLEO were used. Then, our current results with the partial branching ratio, which is 1.1% higher than the PDG result, is reasonable for our somewhat simplistic assumption.

On technical side, we have prepared fitting environment which can be after minor adaptation used for multi-dimensional experimental distributions or other τ decay modes.

²⁵ When looking at the right-hand plot in Fig. 2, the significance of the difference between the model and the data has been computed to be around 4.3 σ in the region from 950 MeV to 990 MeV. The $f_0(980)$ resonance, as opposed to the σ , is included in the $R\chi L$ framework [18] and its (small) contribution to the $\tau^- \rightarrow \pi^- \pi^- \pi^+ \nu_\tau$ decays can with some time be evaluated.

²⁶ The fact that, when σ parameters are unconstrained in the fit, they usually leave the expected physical range hints to such a

possibility. This is especially highlighted by the fact that even in our results, parameter Γ_σ is at its upper limit (see Table I). Fit results for σ parameters seem to depend on minuscule changes in its setup, this may also support conjecture of unphysical nature of σ contribution to the currents or to its inaccurate modeling.

²⁷ Since $M_{a_1(1640)} \sim M_\tau$ the constant width approximation can be used for this resonance.

Acknowledgements

We acknowledge help and discussion with Jakub Zaremba and Sergey Alekhin on numerical details of fitting arrangements. We are also thankful to Alexander Korchin and Pedro Ruiz Femenía for a discussion about the Coloumb interaction and to Rafel Escribano, Bastian Kubis and Jorge Portolés for their comments about the σ meson. Useful discussions with John Michael Roney, Simon Eidelman, Hisaki Hayashii, Denis Epifanov and Swagato Banerjee are acknowledged. We thank members of BaBar collaboration for discussions, in particular William Dunwoodie for discussion of the σ meson. We benefited from discussions with Daniel Gómez Dumm on the determination of the pole parameters of the reso-

nances exchanged in $\tau^- \rightarrow \pi^- \pi^- \pi^+ \nu_\tau$ decays.

This project is financed in part from funds of Polish National Science Centre under decisions DEC-2011/03/B/ST2/00107 and DEC-2011/03/B/ST2/00220. We acknowledge funding from the Alexander von Humboldt-Stiftung/Foundation and the Spanish grant FPA2011-25948 as well. P.R. acknowledges DGAPA for funding his contract and the support of project PAPIIT IN106913. O.S. acknowledges that the final step of this project is financed in part from funds of Foundation of Polish Science grant POMOST/2013-7/12. POMOST Programme is cofinanced from European Union, Regional Development Fund. This project was supported in part by PL-Grid Infrastructure.

-
- [1] O. Shekhovtsova, T. Przedzinski, P. Roig, and Z. Was, Phys.Rev. **D86**, 113008 (2012), 1203.3955.
- [2] O. Shekhovtsova, I. Nugent, T. Przedzinski, P. Roig, and Z. Was, 1301.1964.
- [3] I. M. Nugent, 1301.7105.
- [4] G. Aad et al. (ATLAS), Phys.Lett. **B716**, 1 (2012), 1207.7214.
- [5] S. Chatrchyan et al. (CMS), Phys.Lett. **B716**, 30 (2012), 1207.7235.
- [6] Z. Cyczula, T. Przedzinski, and Z. Was, Eur.Phys.J. **C72**, 1988 (2012), 1201.0117.
- [7] S. Banerjee, J. Kalinowski, W. Kotlarski, T. Przedzinski, and Z. Was, Eur.Phys.J. **C73**, 2313 (2013), 1212.2873.
- [8] J. H. Kuhn and E. Mirkes, Z. Phys. **C56**, 661 (1992).
- [9] E. Aitala et al. (E791), Phys.Rev.Lett. **86**, 770 (2001), hep-ex/0007028.
- [10] J. M.Link *et al.* [FOCUS Collaboration], Phys.Lett.B **585**, 200 (2004), hep-ex/0312040.
- [11] J. Pelaez, Phys.Rev.Lett. **92**, 102001 (2004), hep-ph/0309292.
- [12] I. Caprini, G. Colangelo, and H. Leutwyler, Phys.Rev.Lett. **96**, 132001 (2006), hep-ph/0512364.
- [13] J. Pelaez and G. Rios, Phys.Rev.Lett. **97**, 242002 (2006), hep-ph/0610397.
- [14] F. Yndurain, R. Garcia-Martin, and J. Pelaez, Phys.Rev. **D76**, 074034 (2007), hep-ph/0701025. hep-ph/0701025.
- [15] M. Doring, C. Hanhart, F. Huang, S. Krewald, and U.-G. Meissner, Nucl.Phys. **A829**, 170 (2003), 0903.4337.
- [16] J. Beringer et al.(Particle Data Group) Phys.Rev. **D86**, 01001 (2012) .
- [17] <http://pdg.lbl.gov/2012/reviews/rpp2012-rev-scalar-mesons.pdf>
- [18] V. Cirigliano, G. Ecker, H. Neufeld, and A. Pich, JHEP **0306**, 012 (2003), hep-ph/0305311.
- [19] M. Wagner and S. Leupold, Phys.Lett. **B670**, 22 (2008), 0708.2223.
- [20] L. Geng, E. Oset, J. Pelaez, and L. Roca, Eur.Phys.J. **A39**, 81 (2009), 0811.1941.
- [21] M. Wagner and S. Leupold, Phys.Rev. **D78**, 053001 (2008), 0801.0814.
- [22] A.V. Anisovich and H. Leutwyler, Phys.Lett. **B375**, 335 (1996), hep-ph/9601237.
- [23] F. Niecknig, B. Kubis and S. P. Schneider, Eur. Phys. J. **C72**, 2014 (2012), 1203.2501.
- [24] E. I. Shibata (CLEO), eConf **C0209101**, TU05 (2002), hep-ex/0210039.
- [25] N. A. Tornqvist, Z.Phys. **C68**, 647 (1995), hep-ph/9504372.
- [26] L. D. Landau, V. B. Berestetskii, E. M. Lifshitz, and L. P. Pitaevskii, *Relativistic quantum theory. Course Theor. Phys.* (Pergamon, Oxford, 1971. Trans. from the Russian.).
- [27] D. Gómez Dumm and P. Roig, Eur.Phys.J. **C73**, 258 (2013), 1301.6973.
- [28] D. G. Dumm, P. Roig, A. Pich, and J. Portolés, Phys. Lett. **B685**, 158 (2010), 0911.4436.
- [29] D. GomezDumm, P. Roig, A. Pich, and J. Portolés, Phys. Rev. **D81**, 034031 (2010), 0911.2640.
- [30] I. M. Nugent, SLAC-R-936 (2009).
- [31] B. Aubert et al. (BaBar Collaboration), Phys.Rev.Lett. **100**, 011801 (2008), 0707.2981.
- [32] P. Golonka, T. Pierzchała, E. Richter-Was, Z. Was, and M. Worek, enlarged version of the document hep-ph/0009302, in preparation, to be submitted to Comput. Phys. Commun.
- [33] N. Davidson, G. Nanava, T. Przedzinski, E. Richter-Was, and Z. Was, Comput.Phys.Commun. **183**, 821 (2012), 1002.0543.
- [34] D. Asner et al. (CLEO) Phys.Rev. **D61**, 012002 (2000), hep-ex/9902022.
- [35] I. Antcheva, M. Ballintijn, B. Bellenot, M. Biskup, R. Brun, et al., Comput.Phys.Commun. **180**, 2499 (2009).
- [36] J. H. Kuhn and A. Santamaría, Z. Phys. **C48**, 445 (1990).
- [37] F. James, and M. Roos, Comput.Phys.Commun. **10**, 343 (1975).
- [38] T. Bhattacharya and S. Willenbrock, Phys. Rev. **D47**, 4022 (1993).
- [39] A. Bernicha, G. Lopez Castro and J. Pestieau Phys. Rev. **D50**, 4454 (1994).
- [40] R. Escribano, A. Gallegos, J.L. Lucio, G. Moreno and J. Pestieau, Eur. Phys. Jour. **C28**, 107 (2003), hep-ph/0204338.
- [41] B. Moussallam Eur. Jour. Phys. **C71**, 1814 (2011), 1110.6074.
- [42] R. Garcia-Martin, R. Kaminski, J. R. Pelaez and J. Ruiz de Elvira, Phys. Rev. Lett. **107**, 072001

- ((2011),1107.1635.
- [43] J. A. Oller, Phys. Rev. D **71** 054030 ((2005),hep-ph/0411105.
- [44] A. Pich To appear in Prog.Part.Nucl.Phys., 1310.7922
- [45] D. Boito, R. Escribano, and, M. Jamin, JHEP **1009**, 031 (2010), 1007.1858.
- [46] D. Gómez Dumm, A. Pich, and J. Portolés, Phys. Rev. **D69**, 073002 (2004), hep-ph/0312183.
- [47] T. Coan et al. (CLEO), Phys.Rev.Lett. **92**, 232001 (2004), hep-ex/0401005.
- [48] J. Zaremba, Master Degree Thesis, <http://annapurna.ifj.edu.pl/~jzaremba/>, <https://indico.cern.ch/materialDisplay.py?contribId=42&materialId=slides%&confId=261349>.
- [49] G. Ecker, J. Gasser, A. Pich, and E. de Rafael, Nucl. Phys. **B321**, 311 (1989).
- [50] G. Colangelo, M. Finkemeier, and R. Urech, Phys.Rev. **D54**, 4403 (1996), hep-ph/9604279.